Inhibition Success of a Virtually Created Molecule: Pseudoeriocitrin and Femtomolar Inhibition

Dilara Karaman[1], Ahmet Onur Girişgin[2], Oya Girişgin[2]

1 Yildiz Technical University
2 Bursa Uludağ University

Abstract

Pseudoeriocitrin is a molecule that does not exist in reality but was created *in silico* by assuming the formation of oxygen radicals in eriocitrin and giving a different geometry. It gave femtomolar results during *in silico* docking studies, more successful than eriocitrin in inhibition. This study investigated the reason for this ability of pseudoeriocitrin, an unusual molecule with superior inhibitory activity. This study performed a 3D analysis of possible interactions using the *in silico* protein-ligand docking method. Although it is difficult to say anything definitive, the absence of hydrogen donors renders the pseudoeriocitrin structure highly toxic. This new molecule, which can inhibit various proteins at the femtomolar level such as the lowest K_i value was 3,45 femtomolar, was predicted to be responsible for high binding ability due to its sizeable planar structure and lots of oxygen radicals, which provide many hydrogen bonds with the atoms in the active site of the proteins. It is the first study to show the structure-activity relationship of pseudoeriocitrin via *in silico* dockings. The results indicate that a large core structure, abundant oxygen atoms, planar coordinates, and femtomolar level inhibition are interrelated. The chemical properties resulting from these new biological properties should be examined from various angles. Additionally, more research should be conducted on synthesizing non-radical pseudoeriocitrin.

Dilara KARAMAN[1,a,*], **Ahmet Onur GİRİŞGİN**[2,b], and **Oya GİRİŞGİN**[3,c]

[1] *Bursa Uludağ University, Institution of Natural and App. Science, Biology Department, Bursa-TÜRKİYE*

[2] *Bursa Uludağ University, Veterinary Faculty, Parasitology Department, Bursa-TÜRKİYE*

[3] *Bursa Uludağ University, Karacabey Vocational School, Bursa-TÜRKİYE*

ORCID iD: [a]0000-0003-4386-8531; [b]0000-0002-0020-2708, [c]0000-0001-9896-1093

[*]**Corresponding author:** Dilara KARAMAN, e-mail: dilara.karaman@yahoo.com

Keywords: Eriocitrin, femtomolar inhibition, molecular docking, pseudoeriocitrin.

1. Introduction

In a world in which technological advances in health services have rapidly developed, helminthic infections have remained a severe medical problem. According to recent data, approximately 2 billion people worldwide were infected with at least one species of soil-transmitted helminths (Kamb & Roy, 2023). The frequent recurrence of infections among people living in areas with insufficient sanitation, especially among preschool-aged children, increases the importance of alternative treatments to replace synthetic drugs. Therefore, discovering new anthelmintics with fewer side effects is a very important and challenging task. Oxyurid nematode infections, transmitted orally and frequently recur due to autoinfection, mostly occur in children and cause developmental disorders (Giray and Keskinoğlu, 2006). It was estimated that 400 million people worldwide were infected with *Enterobius vermicularis* in 2015 (Strelkauskas et al., 2015).

β-tubulin, carnitine o-palmitoyltransferase-2, and fumarate reductase are recently focused antinematodal targets for the development of several anthelmintics such as albendazole, mebendazole, ivermectin and thiabendazole. Because the unknown genome sequence and the lack of crystallized structure of the proteins belonged to *Syphacia obvelata*, the homology model of mitochondrial cytochrome c oxidase (COX) proteins can be useful for *in silico* docking experiments in order to investigate the antinematodal properties of some drug candidates against *S. obvelata* (Karaman, 2022).

Performing protein-ligand docking simulations using *in silico* molecular modelling is the initial step towards developing new drugs. These computational experiments can provide researchers with atomic-level information on the interactions between the target and drug molecules. Such experiments are highly valuable in reducing the workload involved in drug development efforts (Yelekçi et al. 2013).

Eriocitrin (2*S*)-2-(3,4-dihydroxyphenyl)-5-hydroxy-7-[(2*S*,3*R*,4*S*,5*S*,6*R*)-3,4,5-trihydroxy-6-[[(2*R*,3*R*,4*R*,5*R*,6*S*)-3,4,5-trihydroxy-6-methyloxan-2-yl] oxymethyl] oxan-2-yl] oxy-2,3-dihydrochromen-4-one is an eriodictyol-derived flavonoid glycosides found mainly in lemon peel and citrus pulp and in plants such as thyme and mint (Inoue et al., 2002). It was formed by the addition of O-β-rutinoside at the 7th position to eriodictyol. It has antioxidant, anti-inflammatory, and antiproliferative properties (Diab et al., 2015; Guo et al., 2019; Miyake et al., 1997). A study by Ferreira et al. reported the presence of eriocitrin and its metabolites in various organs and body fluids in rats administered orange peel extract. Homoeriodictyol and homo-eriodictyol-7-*O*-glucuronide (hERD-7-*O*-Gluc) are the major metabolites of homoeriodictyol, hesperetin and glucuronide metabolites. The half-life of metabolites in blood plasma ranges from 3 to 3.2 hours. Hesperetin-7-*O*- and hesperetin-3'-*O*--gluconic acid, metabolites of eriocitrin, were detected in both tissue and urine of rats. hERD-7-*O*-Gluc reached approximately 8 ng/g in blood plasma 10 hours after administration, and hERD-4'*O*-Gluc reached approximately 2 ng/g after 6 hours, the highest levels in the blood. The gastrointestinal absorption of eriocitrin was very low, and the total bioavailability of eriocitrin was less than 1% (Ferreira et al., 2021).

We investigated the anthelminthic effect of eriocitrin, whose molecular structure is shown in the following figure (Figure 1), in our previous study which yielded *in silico* outcomes (Karaman, 2022). Interestingly, it was found that there was an additional bond in the molecule when studying the possible interactions of eriocitrin with the proteins it inhibits. When this

molecule, called pseudoeriocitrin, and its possible interactions were studied, it was found to inhibit several proteins at the femtomolar level (K_i=10⁻¹⁷mol/L).

The aim of this study was to show the structure and interactions of pseudoeriocitrin, to which it owes its very high score values, possibly related to its anthelmintic activity. *In silico* dockings were significant because docking results have presented information about inhibition potency that could be evaluated for the beginning of a new drug synthesis study. At the same time, these in silico results help drug designers who are interested in the structure-activity relationship of the most potent multi-inhibitors. First time a virtual molecule has been shown with femtomolar inhibition constants against several proteins. Hence its interactions with anthelmintic target proteins researched *in silico* are thoroughly new and original. It is the first study in terms of showing the structure-activity relationship of a multi-radical virtual molecule possessing multi-inhibition ability at very rare K_i values.
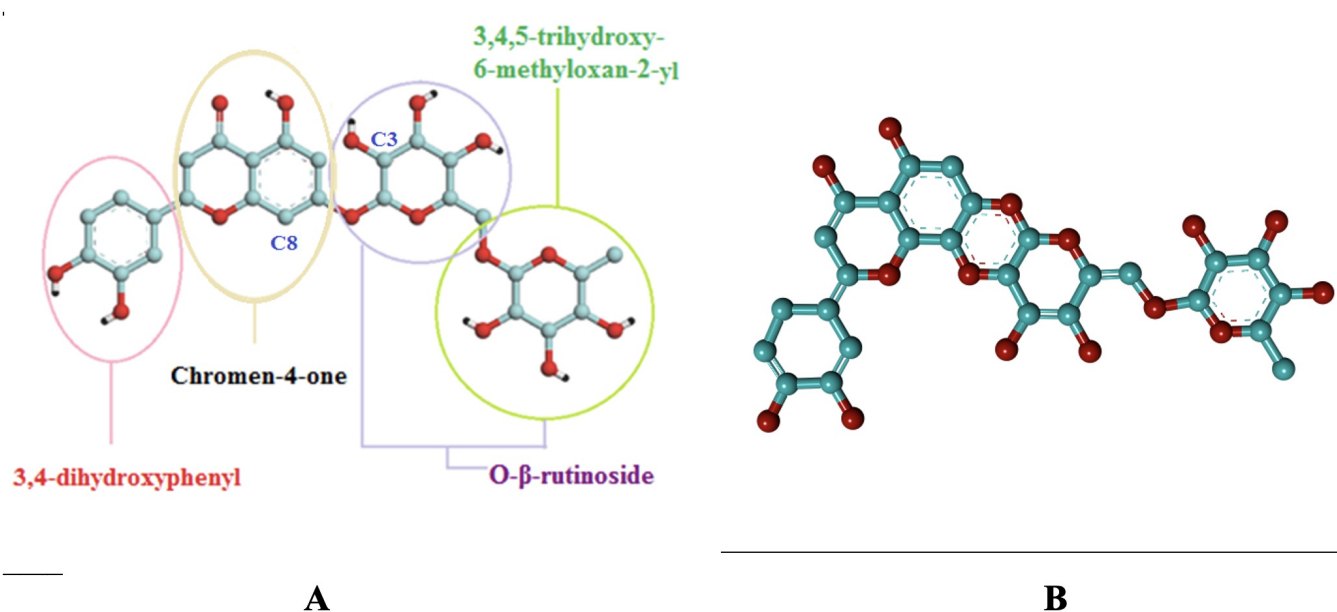
Figure 1. A) Rings forming eriocitrin (original). The bond leading to the formation of pseudoeriocitrin is formed between chromene-4-one ring and the oxygen atom of the hydroxyl group of the chromene-bonded monosaccharide of O-β-rutinoside. **B)** Pseudoeriocitrin.

2. Material and method

2.1. Obtaining and preparation of the ligand

Pseudoeriocitrin was retrieved from the FooDB database (www.foodb.ca) as pdb file in November 2019 (ligand ID: FDB016547). In the pdb file of this molecule, which is deposited in the FooDB database as eriocitrin, all Z coordinates were 0. This pdb file was converted to a pdbqt file using the AutoDock Tool (ADT) (Huey et al., 2007; Morris et al., 2009). When the Z coordinates were 0, the ADT program ignored the hydrogen atoms in the hydroxyl groups and assumed an extra bonding in the core structure because there was sufficient distance between the C8 atom in the chromene ring of

the ligand and the oxygen atom of the hydroxyl group at the C3 position of the rutinositide group to allow bonding (Figure 1). The resulting pdbqt file lacked hydrogen donors. The 3D molecular representation of pseudoeriocitrin is shown in Figure 1.B.

2.2. Preparation of proteins

The proteins and enzymes that could be drug targets in nematodes were chosen. Biovia Discovery Studio 2020 Client (Dassault Systèmes Biovia Inc., 2020) and ADT software were used for protein preparation. For this purpose, target proteins and enzymes found in nematodes and their homologues in humans with their crystallized structures were obtained from the Brookhaven Protein Databank (http://www.rcsb.org/pdb). These target proteins and enzymes are the known targets of anthelmintic drugs such as Albendazole (for beta-tubulin inhibition), Thiabendazole (for fumarate reductase inhibition), and some inhibitors used in *Onchocercha linealis* infection (for carnitine o-palmitoyltransferase inhibition (Taylor et al., 2013)). The homologous proteins which are in humans were used for researching the selectivity of the inhibitor. These proteins were as follows: *Ascaris suum* fumarate reductase enzyme PDB ID: 4YSX (mitochondrial rhodoquinol-fumarate reductase, solubility: 2.25 Å, bound with NN23 inhibitor) (Inaoka et al., 2015), human fumarate reductase enzyme PDB ID: 6VAX (resolution: 2.59 Å) (Sharma et al., 2020); human β-tubulin protein PDB ID: 6E7C (resolution: 3.65 Å) (Ti et al., 2018); *Haemonchus contortus* β-tubulin protein PDB ID: 1OJ0 (in complex with ABZ, theoretical structure) (Robinson et al., 2004); anthelmintic drug target rat carnitine o-palmitoyltransferase PDB ID: 2H4T (resolution: 1.90 Å, bound with dodecane ($C_{12}H_{26}$) (Hsiao et al., 2006) and PDB ID: 2FW3 (resolution: 2.50 Å) (Rufer et al., 2006). We used the work of Taylor et al. (2013) as a reference for the identification of some target proteins. Since the crystallized form of β-tubulin from *Haemonchus contortus* was not available in protein databases, the theoretical structure was used. Ions and ligands, except cofactors and water molecules, were removed. The missing hydrogen atoms were added. The residues of the proteins were checked in terms of missing atoms and bonds. After all hydrogens were added, proteins were optimized, firstly using the "Clean Geometry" tool, followed by the Charm forcefield. After the optimized proteins were saved in pdb format using Discovery Studio 2020 Client, they were opened using ADT to add Gasteiger charges and then saved in pdbqt format. The preparation procedure used by Yelekçi et al. (2013) was followed as a guide for the preparation of proteins.

2.3. Homology modelling

The known protein sequences for *Syphacia obvelata* were searched by using the UniProt Knowledgebase (UniProtKB). Although the cytochrome c oxidase 1 (COX1) and COX2 proteins from the Mt genome are not known targets of anthelmintics, these proteins were selected because they are vital to oxyurid nematodes. Because the genome sequence of *S. obvelata* and the experimental crystal structure of the *Syphacia obvelata* COX1 (SoCOX1) and SoCOX2 proteins are unknown, it was decided to use homology modelling for their 3D structures. Another oxyurid nematode, *Enterobius vermicularis β-tubulin* protein, and *Caenorhabditis elegans* glucose transporter 1 (CeGLUT1) receptor also were *in silico* modelled via homology modelling. Because they are vital for nematodes and potential targets. Homology models and Ramachandran plots are shown in Appendixes. Two different web servers were utilized: the SWISS-MODEL (Waterhouse

et al., 2018) and the Zhang lab I-TASSER web servers (Roy et al., 2010; Yang et al., 2015; Yang and Zhang, 2015) to develop a sequence overlap-based model. The most appropriate 3D structure was preferred by considering Global Model Quality Estimating (GMQE) values and Qualitative Model Energy Analysis (QMEAN) values. For QMEAN, values below 4.0 indicate reliability, while for GMQE, the highest value between 0 and 1 indicates the most reliable predicted structure.

2.4. Docking process

Proteins retrieved from the Protein Data Bank or whose 3D structures were predicted by homology modelling were docked with ligands using AutoDock4.2 (Morris et al., 1998). We determined the grid box size based on the ligand size or the number of torsions. We chose the cofactor of the protein as the centre, or in the absence of a cofactor; we placed the native ligand in the protein into the centre of the grid box. For the beta-tubulin protein docking simulation, the ligand bound to the protein was chosen as the centre. For the CPT enzyme, we referred to the coordinates given by Taylor et al. (2013). The atoms of the protein's active site were allowed to move freely, unlike the other parts of the protein, which were rigid. To dock proteins with their natural ligands in their co-crystallized form, we used their natural ligands as a reference. They set the dielectric constant to 10, the ionic strength to 0.145, the dimensions of the grid box to 60×60×60, and the grid point to 0.375 Å. Since the number of rotational bonds was less than 10, the maximum number of generations was set to 27 000 and the maximum number of extensions to 2 500 000. The docking procedure was performed using the Lamarckian Genetic Algorithm 4.2. AutoDock 4.2 scoring functions were used to generate 10 different conformations for each ligand. After sorting by their free binding energy, the ligands were analyzed for their binding site interactions using AutoDock Tools and Biovia Discovery Studio 2020 Client.

2.5. ADME prediction

SwissADME web server (Daina et al., 2017) was used to estimate the ADME (Absorption, Distribution, Metabolism, Excretion) properties of pseudoeriocitrin and eriocitrin. Their penetration in the blood-brain barrier, gastrointestinal absorption, and oral bioavailability were searched via chemical computation.

Accessing the SwissADME website grants users free and reliable prediction models for various properties including physicochemical characteristics, pharmacokinetics, drug similarity, and medicinal chemistry relevance. These models incorporate credible methods such as BOILED-Egg, iLOGP, and Bioavailability Radar. Lipophilicity, molecular size, polarity, solubility, flexibility, and saturation properties are considered to generate this radar plot (Daina et al., 2017). The six properties in the bioavailability radar are the most basic criteria selected to show whether the physicochemical and pharmacokinetic values expected from a bioavailable compound are within reasonable limits.

According to bioavailability radar, a bioavailable compound should have a molecular weight (MW) between 150-200 g/mol, TPSA between 20-130 $Å^2$, lipophilicity (XLOGP3) between -0.7 and +5.0, carbon fraction in sp3 hybridization, a saturation marker, should not be less than 0. 25 and solubility (log S) not more than 6 (Daina et al., 2017), water solubility score between 1-3 (1, highest solubility, 5, lowest solubility), number of rotatable bonds between 0-9 (Ritchie et al., 2011).

3. Results and Discussion

3.1. Evaluation of possible interactions between pseudoeriocitrin and rat carnitine palmitoyl transferase 2 (CPT 2)

One of the results of this study was that the inhibition constant K_i of pseudoeriocitrin against rat CPT 2 (PDB ID: 2H4T) was 15.83 femtomolar. This result indicates that pseudoeriocitrin may be a very successful CPT 2 inhibitor. However, pseudoeriocitrin can only be used to inform the design of a *de novo* drug candidate molecule, which, in reality, is not accessible in databases.

A study of the possible interactions of pseudoeriocitrin in the rat CPT 2 enzyme-coded 2H4T pdb revealed a large number of interactions with the residues shown in Figure 2 A. Although most of these were apolar amino acids, polar hydrophilic residues such as serenyl and tyrosinyl were located very close to pseudoeriocitrin and TYR486 forms aromatic interactions. Figure 2 B shows that cyclic side chain residues such as PHE131 and PHE134 contribute to hydrogen bond formation rather than aromatic interactions. Five hydrogen bonds were predicted via Biovia 2020 Client (green dashed lines in the figure).
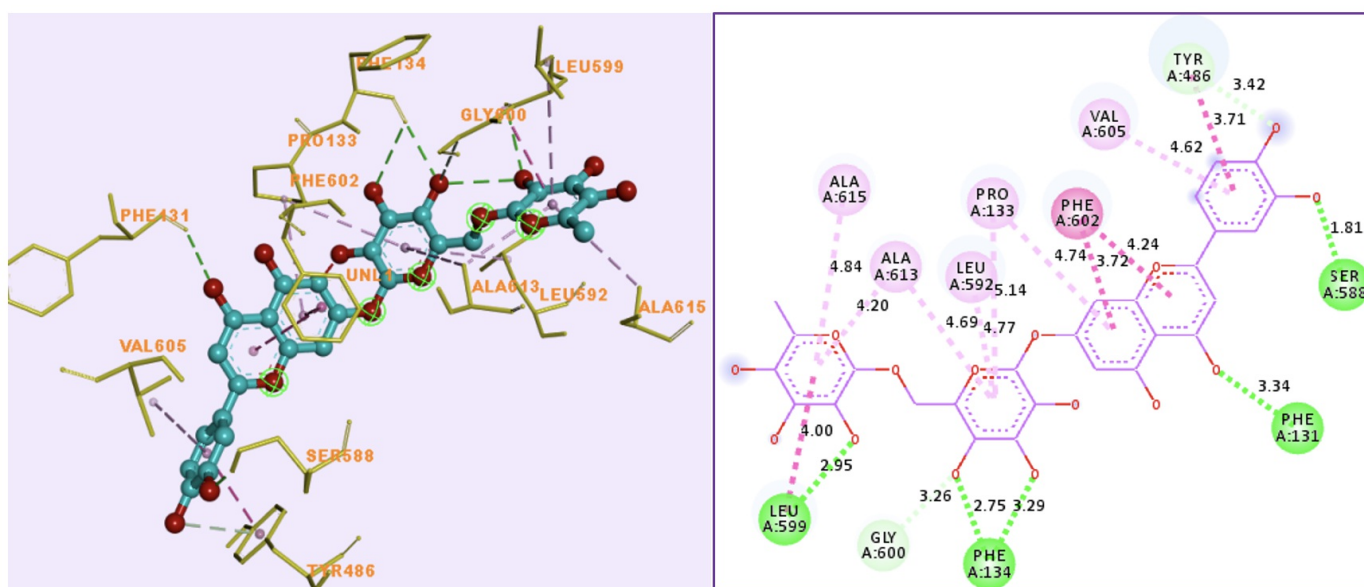

Figure 2. Interactions between pseudoeriocitrin and the rat CPT 2 enzyme. **A)** Carbon atoms of pseudoeriocitrin are illustrated in blue, oxygen atoms in red, and the residues with which it interacts are represented by the yellow stick model. **B)** 2D representation of the interactions between pseudoeriocitrin and the rat CPT 2 enzyme (not shown in the figure because the AutoDock4.2 program does not display the abnormal bond formation in the defective molecule on the coordinate axis of the dlg file).

One of the most important factors in the interactions of pseudoeriocitrin was the chemical attractions emanating from the oxygen atoms on each ring of the ligand. As shown in Figure 2 B, residues LEU599, GLY600, PHE134, PHE131, SER88, and TYR486 formed hydrogen bonds using the oxygen atoms on the ligand. PHE134 formed two hydrogen bonds with the oxygen atoms of the ligand, one at a distance of 2.75 Å and the other at a distance of 3.29 Å, and SER588 formed a
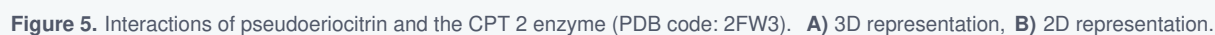
conventional hydrogen bond at a distance of 1.81 Å. PHE602 formed an aromatic interaction with one of the two rings in the center of the ligand and an amide-pi interaction with the other. PRO and ALA residues also formed pi-alkyl interactions with two different rings of the ligand. All rings of the ligand had at least one pi-alkyl interaction.

The hydrophobicity of the region formed by the residues around the pseudoeriocitrin was important because it directly affects the interactions of the ligand. Figure 3 shows the hydrophobic and hydrophilic regions. The presence of some polar residues beyond the hydrophobic surface, caused by the side chains of amino acids such as alanine, valine, glycine, phenylalanine and leucine from the apolar residues surrounding one side of the ligand, caused these parts to be hydrophilic. The surfaces shown in blue in Figure 3 represent the most hydrophilic regions, while the brown surfaces show the hydrophobic regions. The hydrophilic region at the bottom, where tyrosinyl and serinyl residues are located, stands out.
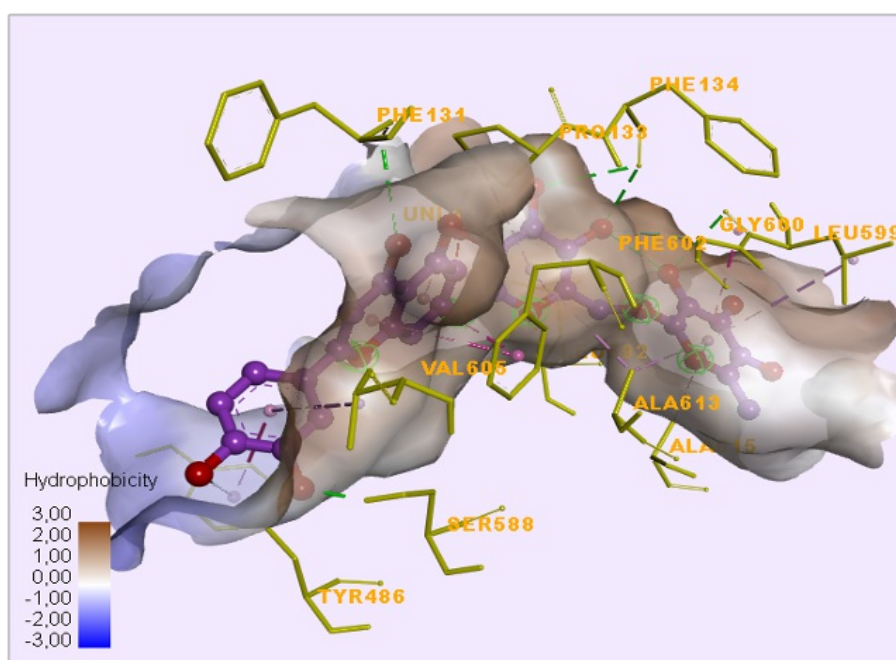
Figure 3. Representation of surface hydrophobicity around pseudoeriocitrin in the binding site of rat CPT 2 enzyme.

To compare the interactions, Figure 4 shows the position of true eriocitrin in rat CPT 2 (2FW3) enzyme and the residues to which it binds. Figure 5 A and B show the different status of pseudoeriocitrin in the same enzyme.

Figure 4. Localization of true eriocitrin in rat CPT-2 enzyme (2FW3).

Figure 5. Interactions of pseudoeriocitrin and the CPT 2 enzyme (PDB code: 2FW3). **A)** 3D representation, **B)** 2D representation.

The video performed to better illustrate the localization of pseudoeriocitrin in the enzyme CPT 2 (2FW3) is in Appendix 1.

Referring to Figure 6 A, which shows the surface of the CPT 2 enzyme and the possible entry site of the ligand, we predicted the cavity (which is shown in orange circle) to be the entry site for the binding site of the enzyme. Figure 6 B

shows pseudoeriocitrin at the site where it binds in the enzyme for comparison.
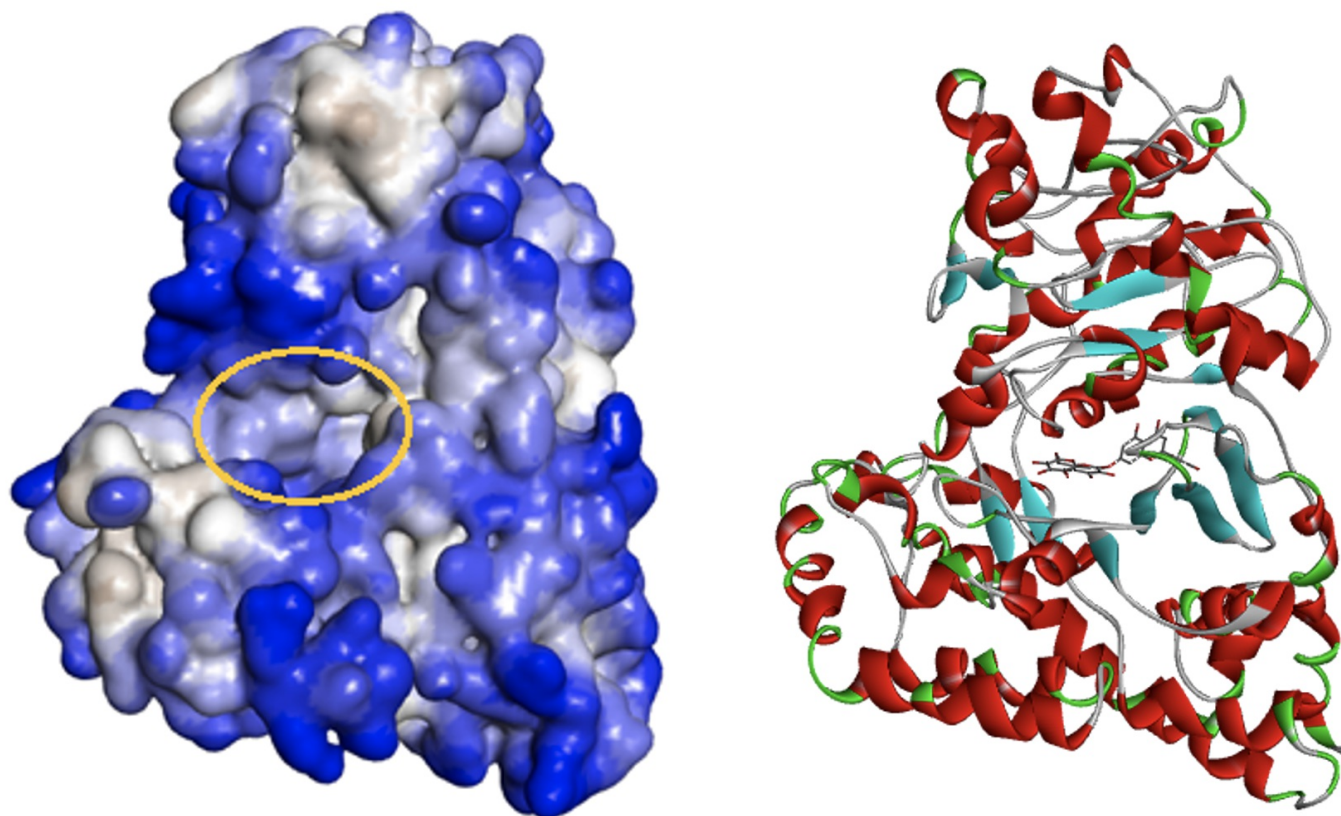

Figure 6. CPT 2 enzyme (2FW3). **A)** In the representation of the enzyme surface, the cavity in the orange circle was presumed to be the entry cavity of pseudoeriocitrin into the enzyme. In the figure, blue regions represent hydrophilic regions and brown regions represent hydrophobic regions. **B)** In this version of the figure in A, shown without a surface, pseudoeriocitrin appears in the centre, in the region of lowest energy, demonstrated with the stick model.

3.2. Evaluation and comparison of possible interactions between pseudoeriocitrin and *Ascaris suum* fumarate reductase (AsFR) and human fumarate reductase (hFR)

Since pseudoeriocitrin binds to AsFR at 512 pMK_i, it also performed very well in the inhibition of this enzyme. The position of pseudoeriocitrin on AsFR and hFR enzymes is shown in Figure 7 and Figure 8. A close look at the figures reveals the bi-oxygenated cyclic structure (ring in the middle of the ligand) that results from the abnormal bond formation and leads to the structure of pseudoeriocitrin. A short video to better understand the localization and interactions of pseudoeriocitrin in hFR can be seen in Appendix 2.

Figure 7. Pseudoeriocitrin, 6VAX, and 4YSX. The pseudoeriocitrin molecules are shown in their positioning within the enzymes AsFR (PDB code: 4YSX) and hFR (PDB code: 6VAX) so that their localization in both different proteins can be compared. AsFR is represented by an orange ribbon and FAD of AsFR by a purple stick model, hFR by a cream ribbon and FAD of hFR by a dark green stick model, pseudoeriocitrin docked to AsFR by a fuchsia ball-stick model, and pseudoeriocitrin docked to hFR by a turquoise ball-stick model.
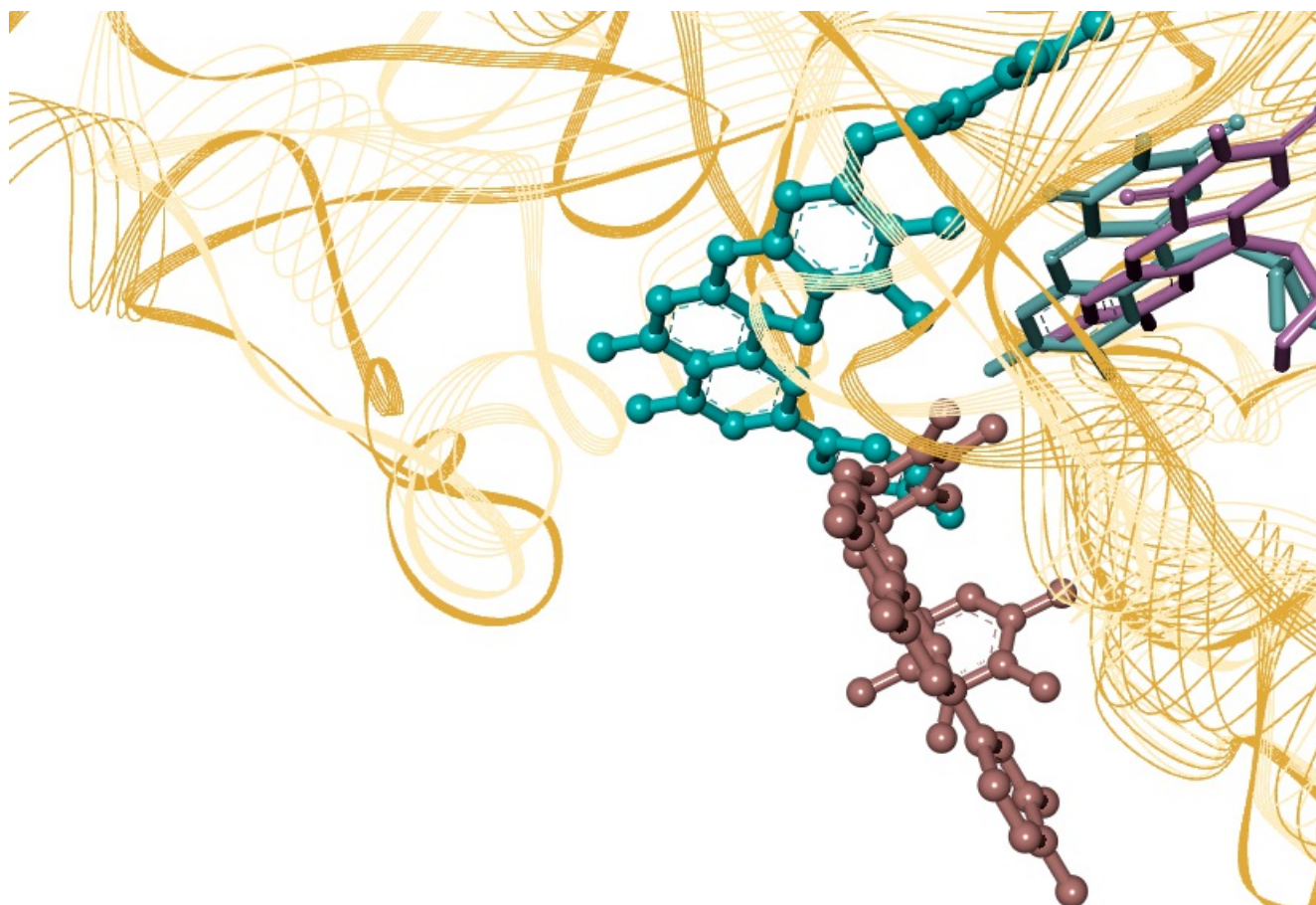
Figure 8. Pseudoeriocitrin are shown in their positioning in hFR and AsFR, FADs are shown in purple and blue with a stick model, the isoalloxazine ring is very close to the pseudoeriocitrin; pseudoeriocitrin are shown in AsFR with a light-pink ball and stick model, and pseudoeriocitrin, represented by the turquoise ball-and-stick model, are shown at the docking points in the hFR where they are located at the lowest energy level.

Possible interactions of pseudoeriocitrin in AsFR are shown in Figure 9 A and B. Hydrogen bond formation was predicted with five different residues. A pi-sigma bond with THR81 is also likely to occur.
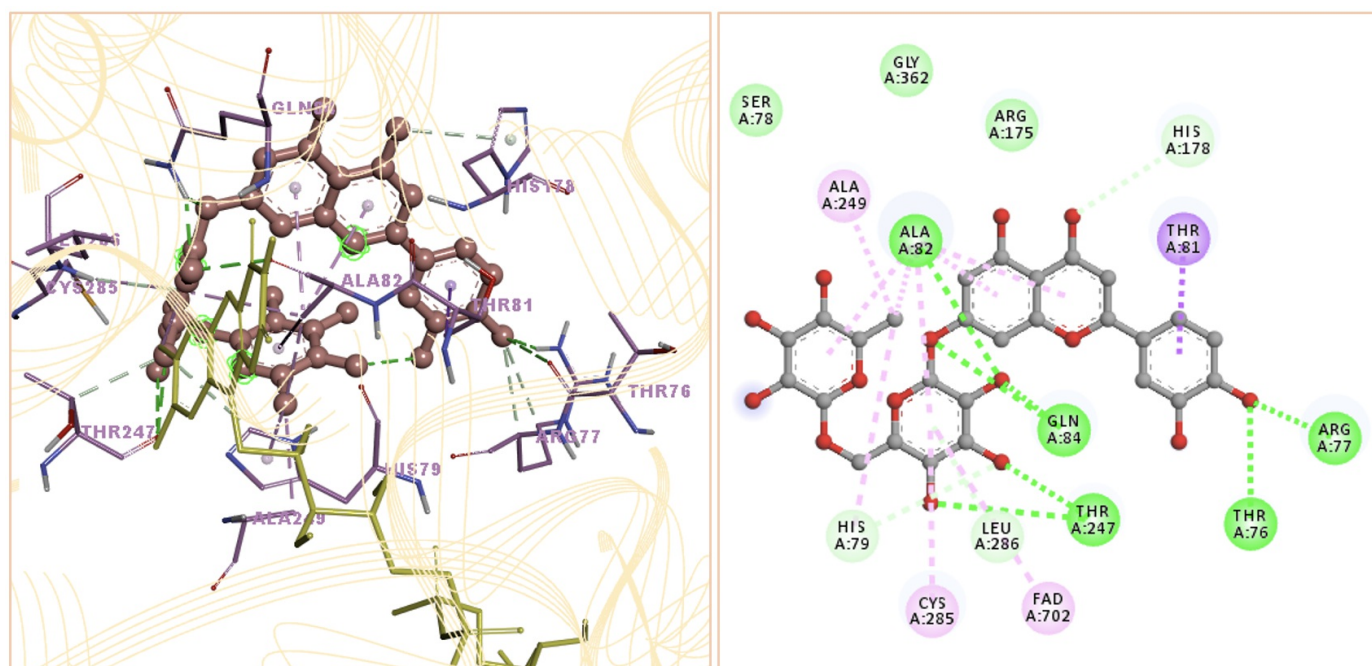
Figure 9. Pseudoeriocitrin and AsFR (4YSX) interactions. **A)** 3D representation, **B)** 2D representation (although the figure shows the eriocitrin structure, it is actually pseudoeriocitrin)

The interactions of pseudoeriocitrin in hFR are shown in Figures 10 A and B, which are used to compare the interactions. We predicted twelve hydrogen bond formations as it has a very good inhibition with 6VAX.
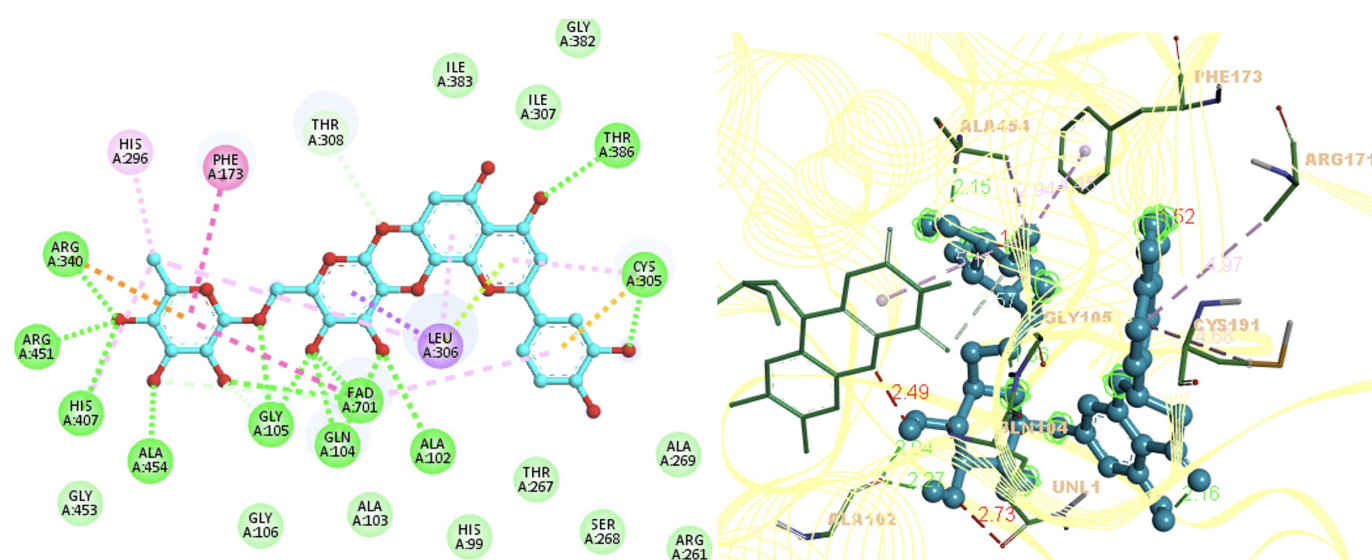
Figure 10. Interactions of pseudoeriocitrin and hFR enzyme (6VAX) **A)** 2D representation shows the faulty bond that leads to the formation of pseudoeriocitrin. The oxygen atom opposite the LEU306 residue, represented by the purple ball in the figure, bonds with chromene to form an abnormal cyclic structure. **B)** 3D representation

3.3. Evaluation of possible interactions between pseudoeriocitrin and *C. elegans* Glucose Transporter 1 (CeGLUT1)

The position of pseudoeriocitrin in CeGLUT1 and the interacting residues are shown in Figure 11 A and B. The docking simulations revealed that pseudoeriocitrin had a very good binding affinity. Although the structure of CeGLUT1 was predicted by homology modeling, we prepared the video in Appendix 3 to show these interactions in more detail since the ΔG value for pseudoeriocitrin was -17.18 kcal/mol. The video shows pseudoeriocitrin with a purple ball and stick model, the protein with a pink ribbon and the residues with a thin stick model.
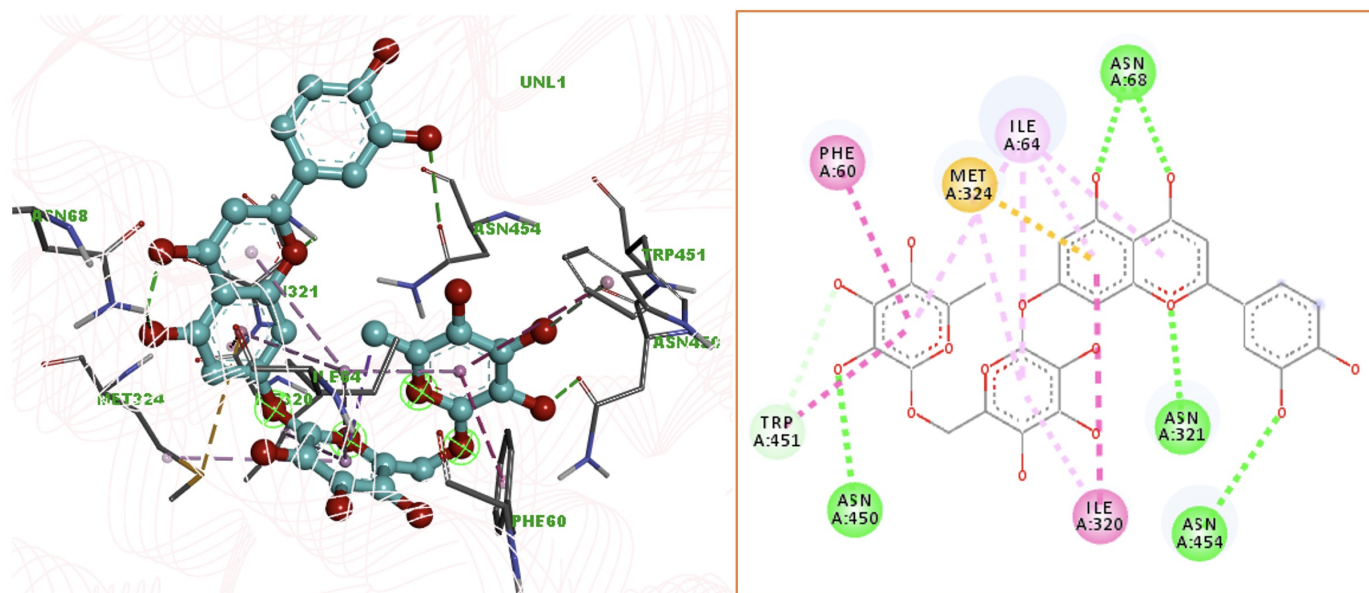

Figure 11. CeGLUT1 interactions with pseudoeriocitrin. **A)** 3D representation of pseudoeriocitrin is represented by the turquoise ball-and-stick model, interacting residues by the thin stick model, and protein by the powdery pink strip ribbon model. **B)** 2D representation of pseudoeriocitrin and CeGLUT1 interactions (the program does not show real pseudoeriocitrin, the ligand in the figure looks like real eriocitrin)

3.4. Pseudoeriocitrin and *Syphacia obvelata* cytochrome c oxidase 1 (SoCOX1) interactions

The ring structure formed by the formation of an extra bond between the chromene ring of pseudoeriocitrin and the rutinoside structure allowed pseudoeriocitrin to interact as shown in Figures 12 A and B. For a better understanding of the interactions with SoCOX1, the short video in Appendix 4 can be viewed.
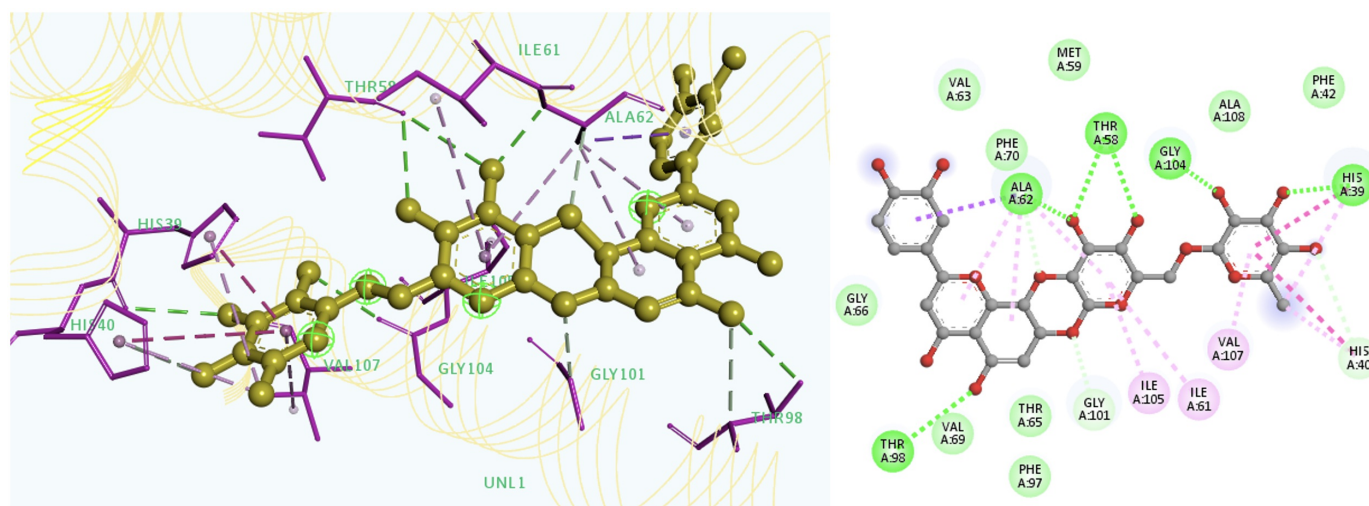
Figure 12. Pseudoeriocitrin and SoCOX1 possible interactions. **A)** Pseudoeriocitrin is represented by a yellow ball and stick, a thin purple stick represents the interacting residues, dashed lines represent the interactions, and the secondary structure of the protein is represented by a cream-colored strip ribbon model. **B)** 2D representation clearly shows the abnormal structure of pseudoeriocitrin

As seen in Figure 12 A, the L-shaped structure formed by the rings of the ligand is strongly attracted by ALA62. In addition, the rhamnosyl ring of the rutinositide group at the other end of the ligand is attracted by the cyclic side groups of residues HIS39 and HIS40 through their aromatic interactions, while VAL107 on another α-helix is attracted to the same group from the opposite direction so that the ligand fits very well to its position. The most important chemical interactions shown in Figure 12 B are the hydrogen bonds formed by HIS39 and GLY104 residues with the oxygen atoms of the ligand. In addition, ALA62 formed six interactions with different points of the ligand. To classify these interactions shown with dashed lines in the figure based on their colors, the purple color represents the pi-sigma bond, the dark green short-distance lines represent hydrogen bonding, the pink lines represent pi-alkyl bonding and the light green long-distance lines represent polar interactions.

3.5. Docking results of pseudoeriocitrin with all proteins

We performed docking experiments with ligands three times. This was due to a structure change in the molecule, which was presumably caused by the optimization procedure. We later realized that the real reason was the presence of erroneous molecules in the FooDB database from which the ligand was taken. In the different molecular structures of pseudoeriocitrin, the formation of oxygen radicals and different geometry gave the molecule a very good score. Table 1 shows the docking results of pseudoeriocitrin. The docking procedure was repeated for pseudoeriocitrin two times (except the first docking with SoCOX1). Different values of the free energy of binding were obtained from dockings at the end of repeated computation.

Table 1. Docking results of Eriocitrin and Pseudoeriocitrin (PE) (ΔG values (kcal/mol))

	1OJ0	2H4T	4YSX	6VAX	SoCOX1	SoCOX2	6E7C	Ev Tub	CeGlut1	2FW3
Eriocitrin	+15.6	-8.43	-6.62	-12.87	-5.92	-3.92	+72.30	+104.9	-6.61	-9.72
PE (in first docking)	-3.21	-18.83	-13.84	-12.30		-8.70	+169.7	+118.6	-8.62	-12.17
PE (in second docking)	+3.67	-18.09	-12.67	-18.45	-16.93	-11.22	+49.1	+52.5	-17.18	-19.73

Table 2. Docking results of Eriocitrin and Pseudoeriocitrin (PE) (*Ki* values)

	1OJ0	2H4T	4YSX	6VAX	SoCOX1	SoCOX2	6E7C	Ev Tub	CeGlut1	2FW3
Eriocitrin	-	663.49 nM	14.13 uM	370,31 pM	45.64 uM	1.34 mM	-	-	14.24 uM	75.23 nM
PE (in first docking)	2270 uM	15.83 fM	71.76 pM	971.51 pM		417.7 nM	-	-	479.82 nM	1.19 nM
PE (in second docking)	-	55.00 fM	512 pM	29.86 fM	389.40 fM	59.4 nM	-	-	257.26 fM	3.45 fM

(PE in the table: Pseudoeriocitrin, fM: femtomolar, Ev Tub:*Enterobius vermicularis* β-tubulin)

According to Table 1, neither eriocitrin nor pseudoeriocitrin could bind to β-tubulin proteins (1OJ0, 6VAX, and EvTub) of any organisms in these searches. Only 1OJ0 (*H. contortus* beta-tubulin) could be inhibited from pseudoeriocitrin but with the very trivial free energy of binding. Therefore, pseudoeriocitrin did not sign a toxic effect in terms of β tubulin binding. On the other hand, β tubulin inhibition is related to stopping cell division. Hence, β tubulin inhibitors have been used both in anthelmintics and anticancer drugs. Pseudoeriocitrin might not be related to blockage of the cell division, but it inhibited some vital enzymes of nematodes such as SoCOX1, SoCOX2, CeGLUT1, and fumarate reductase (4YSX). Hitherto, pseudoeriocitrin can cause cell death in nematodes at very low concentrations that might be tolerated in the human body via radical scavenging and the immune system.

The selectivity index was calculated as 152542,4 for *S. obvelata* COX1 (SoCOX1) enzyme to SoCOX2 enzyme with pseudoeriocitrin based on the K_i values. Both of these enzymes' 3D structures were predicted with homology modelling via the SwissModel web server. According to this *in silico* approach, pseudoeriocitrin was more effective on SoCOX1 inhibition rather than SoCOX2 enzymes.

Figure 13 A, B, and C show the SwissADME results for this molecule.
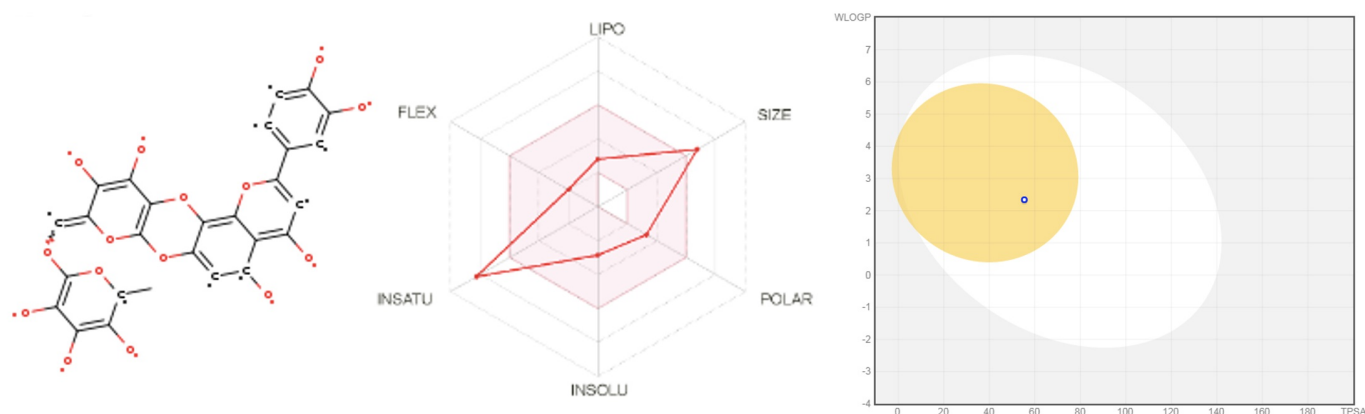
Figure 13. SWISSADME result of pseudoeriocitrin. **A)** Molecular structure of pseudoeriocitrin, **B)** radar plot, **C)** ability to penetrate the blood-brain barrier.

Interestingly, this molecule was predicted at first to penetrate the blood-brain barrier, be well absorbed in the gastrointestinal tract, and bind to some cytochrome enzymes that are not inhibited by eriocitrin (SwissADME results for pseudoeriocitrin were shown in Appendixes). In the second research for the same molecule, SWISSADME webserver did not accept to predict since the molecular weight is more than 500 g/mol. The most significant point was seen in Figure 13 A that pseudoeriocitrin is a multiradical. This radical structure is also related to toxicity and binding ability. However, this molecule (pseudoeriocitrin) searched in ZincDatabase is not present in the database. The interactions associated with pseudoeriocitrin are intended to be used in the discovery of a new anthelmintic based on its very favorable binding of free energies.

Amić et al. (2014) showed that a new bond can be formed in the morin molecule by calculating and comparing the enthalpy that enables the conformational change required to form an intramolecular bond. This new conformation of morin gives the molecule the ability to increase its radical scavenging activity while making it planar. Morin is also a flavone, and the prospective binding results in a planar extension of the flavone core, i.e., the formation of a ring parallel to the core plane. This is the same condition as the flavone structure in our study. The bond formation between the flavone core and the rutinozide group increases the planar area consisting of cyclic structures. This allows the hydroxyl groups of the molecule to form a large number of hydrogen bonds with the protein, resulting in an increased inhibitory effect.

Brown et al. (2000) predicted that some modifications of the inhibitor mupirocin could enhance the inhibition of isoleucyl-t-RNA synthetase. Indeed, the new inhibitors based on modified mupirocin combined with an amino acid side chain inhibited the enzyme isoleucyl-tRNA synthetase with 10 and 12 femtomolar K_d values, whereas the parent compound inhibited the same enzyme with 140 pM K_d values. When considered as a modified form of eriocitrin in the present study, pseudoeriocitrin appears to be much more favourable than eriocitrin in terms of efficacy. However, the fact that pseudoeriocitrin has a very high binding affinity for some proteins tested in this study suggests that it would be an extremely toxic molecule.

If Pseudoeriositrin's femtomolar inhibition value is due to a chemical reason, we think that this amazing inhibition ability may be due to the following properties:

1. The heterocyclic center structure has a planar geometry.

2. The core structure of the ligand (the combined cyclic structures in the centre) is wide and consists of four rings.

3. Side chains attached to the core have hydroxyl groups or oxygen atoms.

4. Positioning of 3,4,5-trihydroxy-6-methyloxan-2-yl and 3,4-dihydroxyphenyl groups perpendicular to the core plane.

5. The center of the ligand is rigid in a wide area and the side groups are connected to the heterocyclic center via sigma bonds.

The fact that radical oxygen atoms on pseudoeriocitrin are responsible for a number of hydrogen bonds, it should be researched whether normal double-bonded oxygen atoms instead of radical oxygen atoms could create the same inhibition effect.

4. Conclusion

Further exploration is necessary to ascertain whether this molecule can be produced endogenously or synthetically. Pseudoeriocitrin exhibits a remarkable ability to inhibit various enzymes at exceedingly low concentrations without forming covalent bonds, even if only it is produced for a brief period. Therefore, it is essential to pursue this investigation to validate the efficacy and safety of pseudoeriocitrin. Furthermore, this study has gained new insights about an exceptional inhibitor that can effectively inhibit at the femtomolar level. This discovery can be essential in the understanding of structure-activity relationship of most potent inhibitors in the future. The first time, this study illustrated the magnificent inhibition properties of a multi-radical molecule possessing a tetracyclic core structure *in silico*.
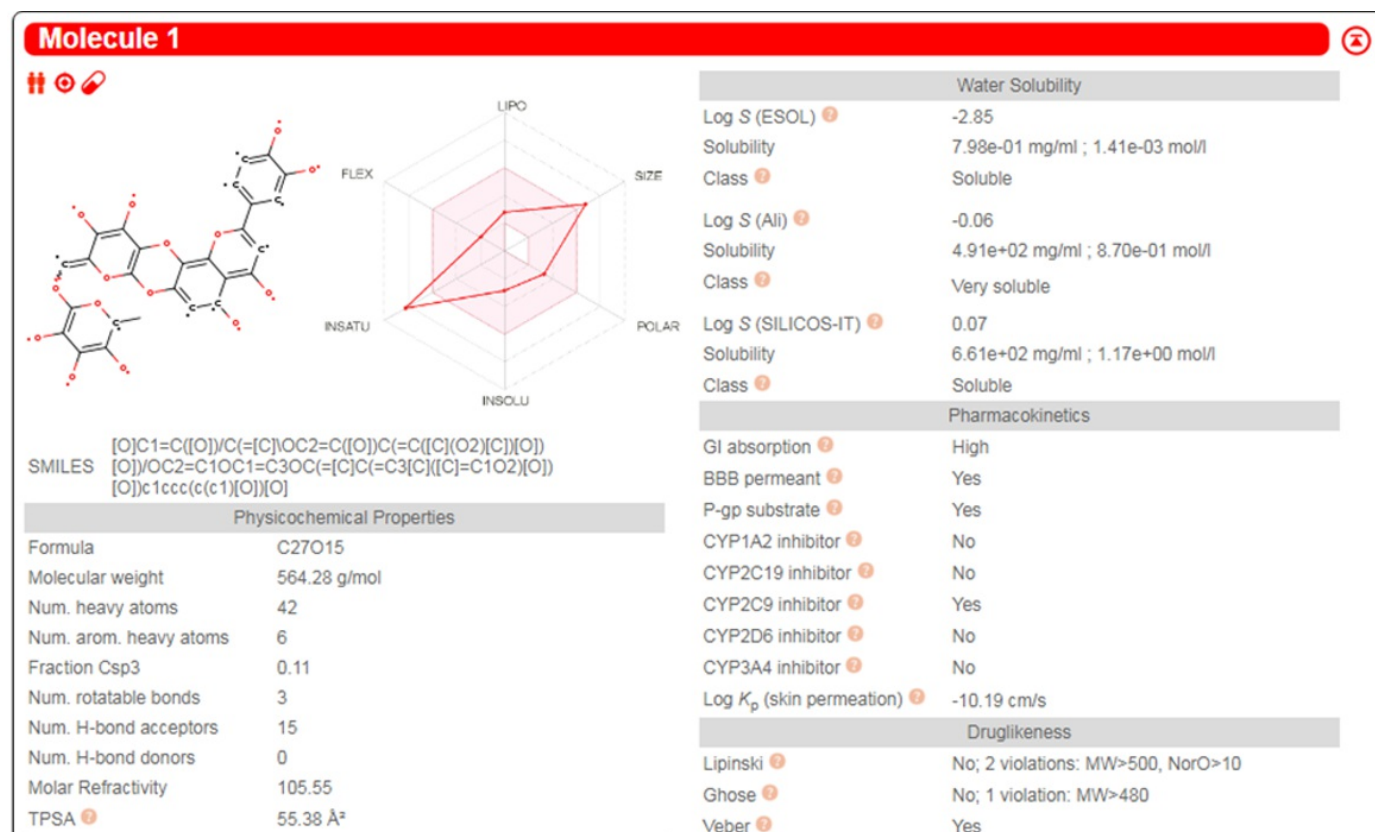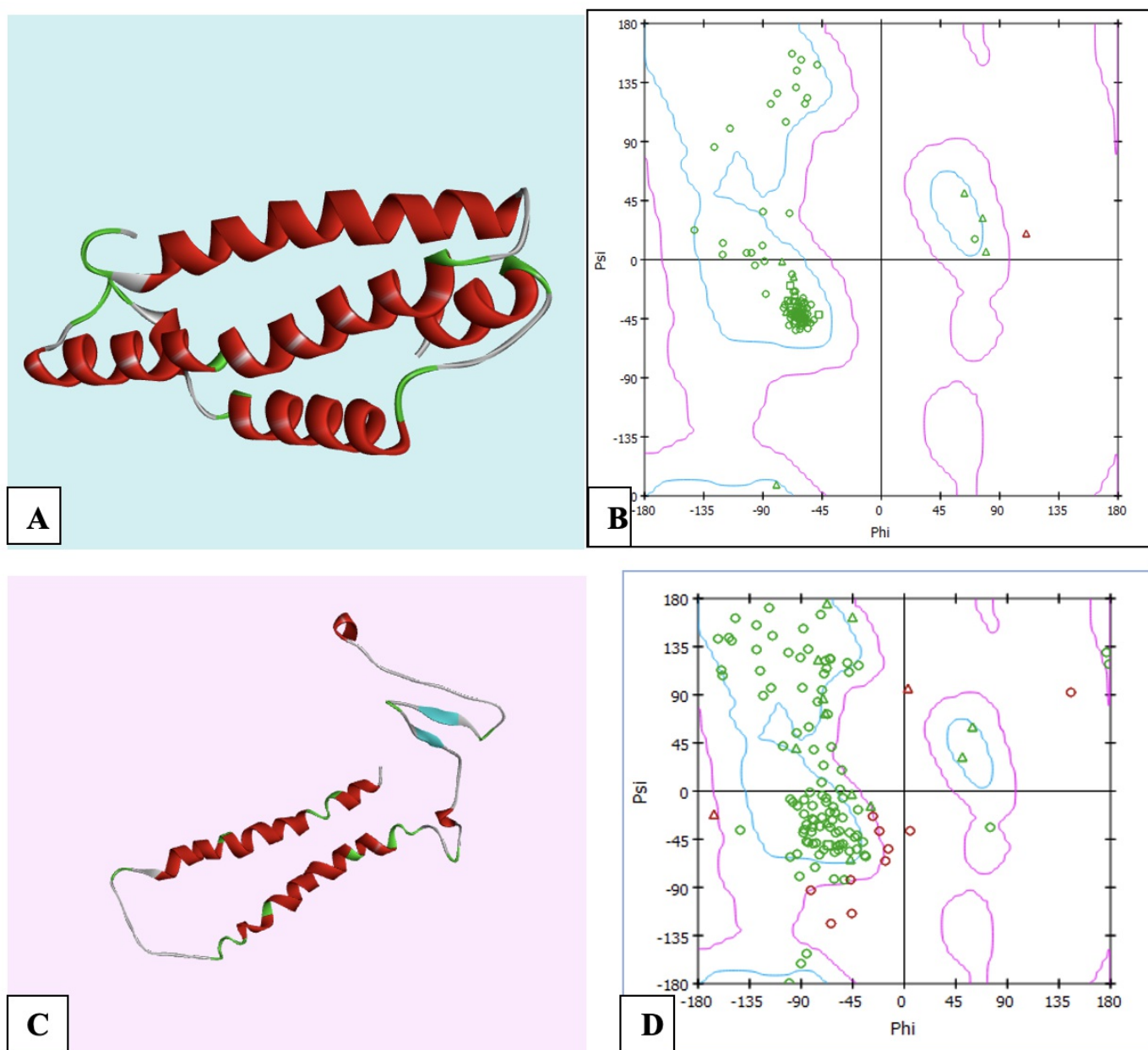
Appendixes

Molecule 1

SMILES [O]C1=C([O])/C(=[C]\OC2=C([O])C(=C([C](O2)[C])[O]) [O])/OC2=C1OC1=C3OC(=[C]C(=C3[C]([C]=C1O2)[O]) [O])c1ccc(c(c1)[O])[O]

Physicochemical Properties

Formula	C27O15
Molecular weight	564.28 g/mol
Num. heavy atoms	42
Num. arom. heavy atoms	6
Fraction Csp3	0.11
Num. rotatable bonds	3
Num. H-bond acceptors	15
Num. H-bond donors	0
Molar Refractivity	105.55
TPSA	55.38 Å²

Water Solubility

Log S (ESOL)	-2.85
Solubility	7.98e-01 mg/ml ; 1.41e-03 mol/l
Class	Soluble
Log S (Ali)	-0.06
Solubility	4.91e+02 mg/ml ; 8.70e-01 mol/l
Class	Very soluble
Log S (SILICOS-IT)	0.07
Solubility	6.61e+02 mg/ml ; 1.17e+00 mol/l
Class	Soluble

Pharmacokinetics

GI absorption	High
BBB permeant	Yes
P-gp substrate	Yes
CYP1A2 inhibitor	No
CYP2C19 inhibitor	No
CYP2C9 inhibitor	Yes
CYP2D6 inhibitor	No
CYP3A4 inhibitor	No
Log K_p (skin permeation)	-10.19 cm/s

Druglikeness

Lipinski	No; 2 violations: MW>500, NorO>10
Ghose	No; 1 violation: MW>480
Veber	Yes

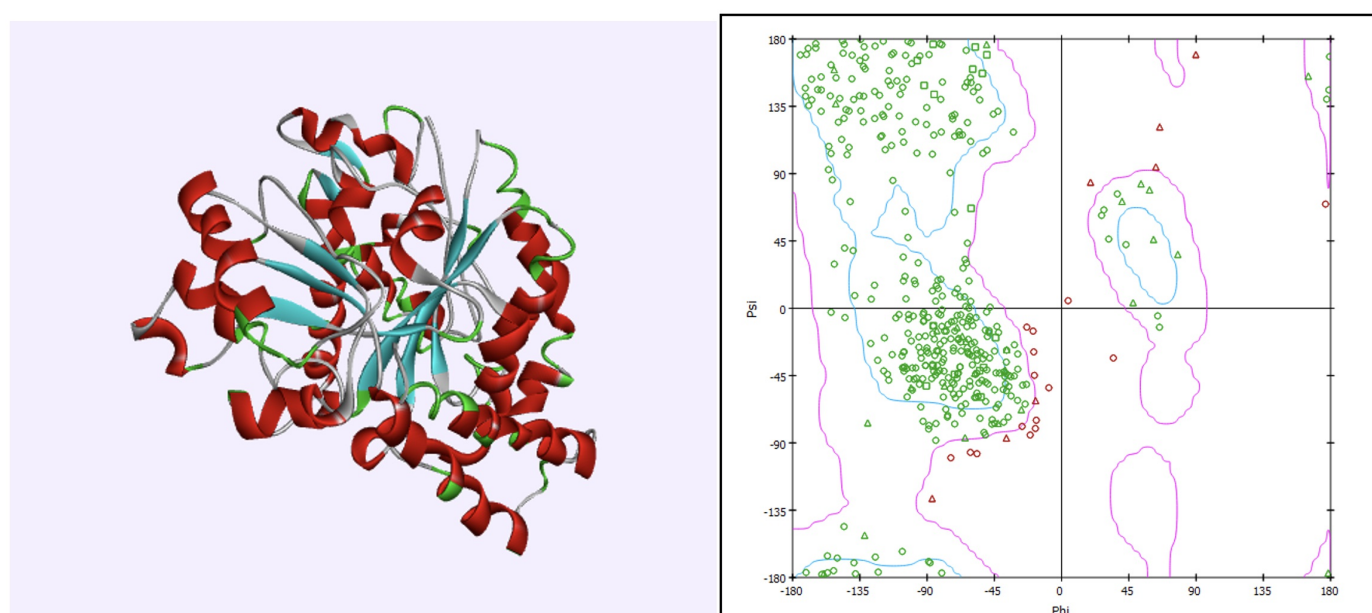**Figure App-1.** SwissADME result of pseudoeriocitrin

Figure App-2. SoCOX1 and SoCOX2. **A)** Homology model of *S. obvelata* COX1 (cytochrome c oxydase 1) enzyme (SoCOX1). **B)** Ramachandran plot for SoCOX1 **C)** Homology model ofSoCOX2 **D)** Ramachandran plot for SoCOX2.
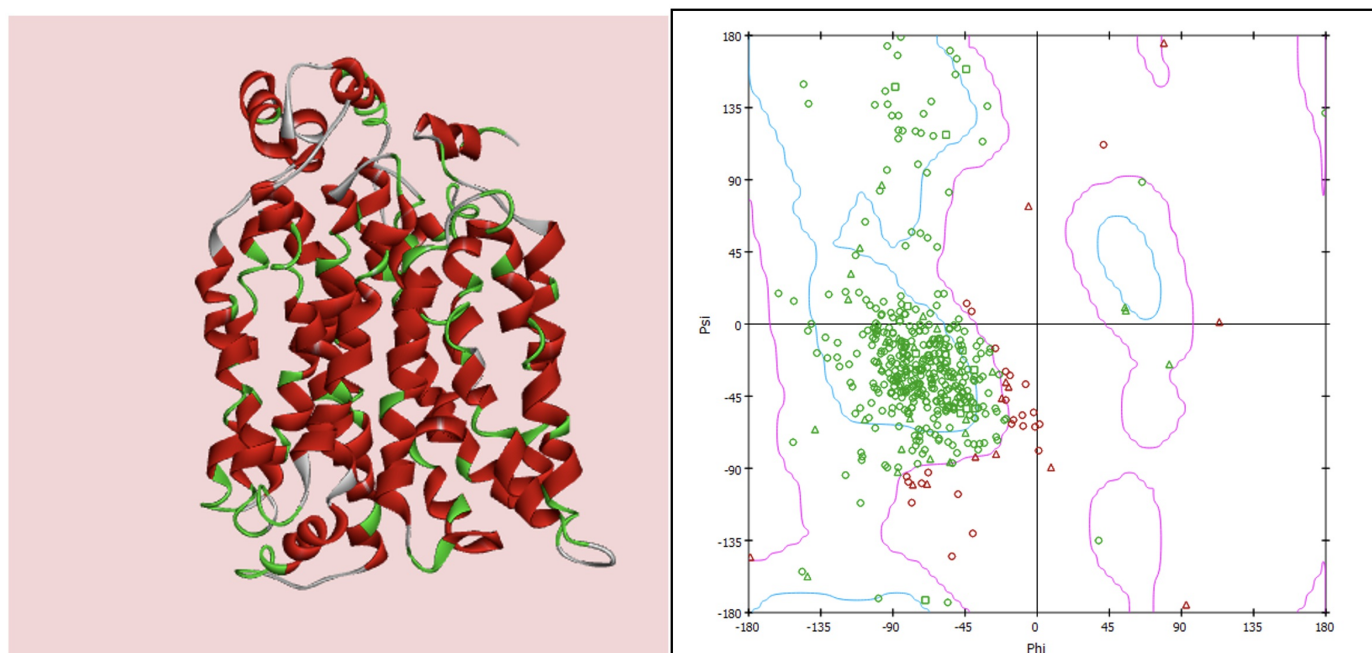
Figure App-3. CeGLUT1. **A)** Homology model of *Caenorhabditis elegans* (CeGLUT1) **B)** Ramachandran plot for CeGLUT1

Figure App-4. Evβ-tubulin. **A)** Homology model of *E. vermicularis* β-tubulin protein **B)** Ramachandran plot for Evβ-tubulin

Statements and Declarations

Acknowledgements

Conflict of interest

The authors declare that there is no conflict of interest.

Research and Publication Ethics

The authors declare that this study complies with research and publication ethics.

References

- Amić, A., Marković, Z., Dimitrić Marković, J. M., Stepanić, V., Lučić, B., Amić, D. (2014). Towards an improved prediction of the free radical scavenging potency of flavonoids: the significance of double PCET mechanisms. *Food Chemistry,* 152, 578-585. doi: 10.1016/j.foodchem.2013.12.025.

- Brown, M. J., Mensah, L. M., Doyle, M. L. Broom, N. J., Osbourne, N., Forrest, A. K., Richardson, C.M., O'Hanlon, P. J., Pope, A. J. (2000). Rational design of femtomolar inhibitors of isoleucyl tRNA synthetase from a binding model for pseudomonic acid-A. *Biochemistry,* 39(20), 6003-6011. doi: 10.1021/bi000148v.

- Daina, A., Michielin, O., Zoete, V. (2017). SwissADME: a free web tool to evaluate pharmacokinetics, drug-likeness and medicinal chemistry friendliness ofsmall molecules, *Scientific Reports,* 7, 42717.

- Dassault Systèmes BIOVIA, Discovery Studio Modeling Environment, Release 2020, San Diego.

- Diab, K. A. E., Shafik, R. E., Yasuda, S. (2015). In vitro Antioxidant and Antiproliferative Activities of Novel Orange Peel Extract and and It's Fractions in Leukemia HL-60 Cells. *Asian Pacific Journal of Cancer Prevention,* 16(16), 7053-7060.

- Ferreira, P. S., Manthey, J. A., Nery, M. S., Cesar, T. B. (2021). Pharmacokinetics and Biodistribution of Eriocitrin in Rats. *Journal of Agricultural Food Chemistry,* 69(6), 1796-1805. doi: 10.1021/acs.jafc.0c04553.

- Giray, H., Keskinoğlu, P. (2006). Ilkokul öğrencilerinde *Enterobius vermicularis* varliği ve etkileyen etmenler [The prevalence of *Enterobius vermicularis* in schoolchildren and affecting factors]. *Turkiye parazitolojii dergisi,* 30(2), 99–102. Retrieved from: http://cms.galenos.com.tr/Uploads/Article_22736/TPD-30-99.pdf

- Guo, G., Shi, W., Shi, F., Gong, W., Li, F., Zhou, G., She, J. (2019). Anti-inflammatory effects of eriocitrin against the dextran sulfate sodium-induced experimental colitis in murine model. *Journal of Biochemical Molecular Toxicology,* 33(11), e22400.

- Hsiao, Y. S., Jogl, G., Esser, V., Tong, L. (2006). Crystal structure of rat carnitine palmitoyltransferase II (CPT-II). *Biochemical and biophysical research communications,* 346(3), 974–980. https://doi.org/10.1016/j.bbrc.2006.06.006

- Huey, R., Morris, G. M., Olson, A. J., Goodsell, D. S. A. (2007). Semiempirical Free Energy Force Field with Charge-Based Desolvation. *Journal of Computational Chemistry,* 28, 1145-1152.

- Inaoka, D. K., Shiba, T., Sato, D., Balogun, E. O., Sasaki, T., Nagahama, M., … Harada, S. (2015). Structural Insights into the Molecular Design of Flutolanil Derivatives Targeted for Fumarate Respiration of Parasite Mitochondria. *International journal of molecular sciences,* 16(7), 15287–15308. https://doi.org/10.3390/ijms160715287

- Inoue, T., Sugimoto, Y., Masuda, H., Kamei, C. (2002). Antiallergic effect of flavonoid glycosides obtained from Mentha piperita. *Biological and Pharmaceutical Bulletin,* 25, 256-259.

- Kamb, M., Roy, S. (2023). Helminths, Soil-Transmitted. Travel-Associated Infections & Diseases, CDC Yellow Book 2024, Page last reviewed: May 01, 2023, Retrieved from: https://wwwnc.cdc.gov/travel/yellowbook/2024/infections-diseases/helminths-soil-transmitted

- Karaman, D. (2022). Prediction on the Anthelmintic Effects of Some Herbal Ligands and Their Derivatives with *In Silico* Molecular Modelling Method, Doctoral Thesis, Bursa Uludag University, 421p, Bursa, Türkiye.

- Miyake, Y., Yamamoto, K., Osawa, T. (1997). Isolation of eriocitrin (Eriodictyol 7-rutinoside) from lemon fruit (*Citrus limon* BURM. F.) and its antioxidative activity. *Food Science Technology International Tokyo*, 3(1), 84-89.

- Morris, G. M., Huey, R., Lindstrom, W., Sanner, M.F., Belew, R. K., Goodsell, D. S., Olson, A. J. (2009). Autodock4 and AutoDockTools4: Automated docking with selective receptor flexibility. *Journal of Computatioanl Chemistry,* 30, 2785–2791.

- Morris, G. M., Goodsell, D. S., Halliday, R. S., Huey, R., Hart, W. E., Belew, R. K., Olson, A.J. (1998). Automated Docking using a Lamarckian Genetic Algorithm and an Empirical Binding Free Energy Function. *Journal of Computational Chemistry,* 19, 1639-1662.

- Ritchie, T. J., Ertl, P., Lewis, R. (2011). The graphical representation of ADME-related molecule properties for medicinal chemists. *Drug Discov Today,* 16, 65–72.

- Robinson, M.W., McFerran, N., Trudgett, A., Houy, L, Fairweather, I. (2004). A possible model of benzimidazole binding to beta-tubulin disclosed by invoking an inter-domain movement. *Journal of Molecular Graphics and Modelling,* 23(3), 275-84. doi: 10.1016/j.jmgm.2004.08.001.

- Roy, A., Kucukural, A., Zhang, Y. (2010). I-TASSER: a unified platform for automated protein structure and function prediction. *Nature Protocols,* 5, 725-738. https://zhanggroup.org/papers/2010_3.pdf

- Rufer, A. C., Thoma, R., Benz, J., Stihle, M., Gsell, B., De Roo, E., … Hennig, M. (2006). The crystal structure of carnitine palmitoyltransferase 2 and implications for diabetes treatment. *Structure (London, England: 1993)*, 14(4), 713–723. https://doi.org/10.1016/j.str.2006.01.008

- Sharma, P., Maklashina, E., Cecchini, G., Iverson, T. M. (2020). The roles of SDHAF2 and dicarboxylate in covalent flavinylation of SDHA, the human complex II flavoprotein. *Proceedings of the National Academy of Sciences of the United States of America,* 117, 23548-23556. https://doi.org/10.1073/pnas.2007391117

- Strelkauskas, A., Edwards, A., Fahnert, B., Pryor, G., Strelkauskas, J. (2015). *Microbiology: A Clinical Approach.* NY, USA: Garland Science. https://doi.org/10.1201/9780429258701

- Taylor, C. M., Wang, Q, Rosa, B. A., Huang, S. C.-C., Powell, K., Schedl, T., … Mitreva, M. (2013). Discovery of Anthelmintic Drug Targets and Drugs Using Chokepoints in Nematode Metabolic Pathways. *PLOS Pathogens,* 9(8), 1003505. doi:10.1371/journal.ppat.1003505

- Ti, S. C., Alushin, G. M., Kapoor, T. M. (2018). Human β-Tubulin Isotypes Can Regulate Microtubule Protofilament Number and Stability. *Developmental cell*, 47(2), 175–190.e5. https://doi.org/10.1016/j.devcel.2018.08.014

- Waterhouse, A., Bertoni, M., Bienert, S., Studer, G., Tauriello, G., Gumienny, R., … Schwede, T. (2018). SWISS-MODEL: homology modelling of protein structures and complexes. *Nucleic acids research*, 46(W1), W296–W303. https://doi.org/10.1093/nar/gky427

- Yang, J., Yan, R., Roy, A., Xu, D., Poisson, J., Zhang, Y. (2015). The I-TASSER Suite: Protein structure and function

prediction. *Nature Methods,* 12, 7-8 https://zhanggroup.org/papers/2015_1.pdf

- Yang, J., Zhang, Y. (2015). I-TASSER server: new development for protein structure and function predictions.*Nucleic Acids Research,* 43, 174-181. doi: 10.1093/nar/gkv342
- Yelekçi, K., Büyüktürk, B., Kayrak, N. (2013). In silico identification of novel and selective monoamine oxidase B inhibitors. *Journal of Neural Transmission (Vienna),* 120(6), 853-858.